Applied Thermal Engineering 219 (2023) 119467

Contents lists available at ScienceDirect

Applied Thermal Engineering

journal homepage: www.elsevier.com/locate/apthermeng

Research Paper

Analytical solution for heat and mass transfer in desiccant coated heat exchangers

Ali Rahnama [a], Mohammad Amani [b], Majid Bahrami [a,*]

[a] Laboratory for Alternative Energy Conversion (LAEC), School of Mechatronic Systems Engineering, Simon Fraser University, BC V3T 0A3, Canada
[b] Department of Mechanical Engineering, Arak University of Technology, Arak, Iran

ARTICLE INFO

Keywords:
Desiccant-coated heat exchanger
Dehumidification coefficient of performance (DCOP)
Moisture removal capacity (MRC)
Analytical solution
Experimental study

ABSTRACT

Due to the complicated nature of desiccant-coated heat exchangers (DC-HXs), solving the highly-coupled transient heat and mass transfer equations using numerical simulations are rather time-consuming and as a result may be impractical for real-time system optimization and seasonal simulations. On the other hand, the approach of majority of studies associated with DC-HXs is numerical and experimental analyses and there is no analytical model that can accurately predict the heat and moisture transfer in a DC-HX in the literature. Thus, in this paper, a new closed-form analytical solution is proposed to accurately predict the heat and moisture transfer in a DC-HX for the first time. The governing equations are simplified to a set of linear ordinary differential equations with initial conditions and then solved analytically. In the present analytical model, both linear and exponential profiles are assumed for the air temperature and humidity ratio along the DC-HX and the results are compared to experimental data collected in our lab. A new DC-HX coated with AQSOA™-FAM-Z02 is also fabricated and tested in our custom-built testbed under a wide range of operating conditions for model validation and performance assessment. Our results indicate that the present analytical solution with exponential profile assumption predicts the experimental data with an average relative difference of less than 10 %, while the linear profile assumption results in a relative difference of ~ 20 % with the experimental data. The new analytical solution is capable of predicting the performance of DC-HXs, which is crucial for design, optimization and operating dehumidification systems in a variety of applications.

1. Introduction

Human thermal comfort is attained by controlling indoor air quality parameters, including temperature, relative humidity (RH), and air velocity. Humidity control is an essential function of heating, ventilation, and air conditioning (HVAC) systems. More importantly, when air moisture content exceeds a certain level in a building, it can result in fungus growth that can lead to serious health issues, particularly respiratory diseases. The need for proper ventilation and humidity control becomes more acute in northern cold climates such as Canada, where people spend most of the cold season in indoor spaces. As such, Northern Canada, Alaska and Greenland have the highest rate of respiratory infections in infants [1]. The reason is energy saving strategies that recommend air tight building construction in northern climates, resulting in insufficient fresh air ventilation, humidity build-up, and indoor mold growth [2–4]. Based on a study performed in Nunavut (Northern Canada), the main cause of respiratory infections is insufficient ventilation rate (~20 m^3/h) [5]. Minimum required ventilation rate could be calculated based on ASHRAE standards, e.g. 75 m^3/h for a 70 m^2 single-bedroom apartment [6].

To provide the required air quality, mechanical and desiccant dehumidification systems are the commonly-used systems for indoor humidity control [7]. Mechanical dehumidification systems, such as vapor compression refrigeration systems cool the air stream below its dew point to extract the air water content, thereby removing the latent load. On the other hand, desiccant dehumidification systems rely on the absorption or adsorption of water vapor using desiccant materials. In this method, the latent load and sensible heat can be removed using thermal energy (waste-heat) as oppose to electrical energy used in mechanical dehumidification systems. In addition, there are membrane-based enthalpy recovery ventilator (ERV) systems that provide fresh air and ventilation in buildings, see Ref. [8–10] for more information, however; ERV application in cold climate may be problematic due to potential membrane freezing issues.

Waste-heat driven solid-desiccant dehumidification systems, see

* Corresponding author.
E-mail addresses: m.amani@arakut.ac.ir (M. Amani), mbahrami@sfu.ca (M. Bahrami).

https://doi.org/10.1016/j.applthermaleng.2022.119467
Received 21 May 2022; Received in revised form 23 September 2022; Accepted 9 October 2022
Available online 17 October 2022

Nomenclature

c_p	Specific heat capacity (J/kg.K)
H	Channel height (m)
h	convective heat transfer coefficient(w/m^2.K)
h_{ad}	Enthalpy of adsorption (J/kg)
h_m	convective mass transfer coefficient (m/s)
Nu	Nusselt number (-)
k	Thermal conductivity (W/m.K)
L	length of channel(m)
RH	Relative humidity (-)
P	Pressure (Pa)
T	Temperature (K)
t	time (s)
u	Air velocity (m/s)
W	uptake of desiccant (kg/kg)
x	Axial direction (m)
y	Radial direction (m)

Greek parameters

ρ	Density (kg/m^3)
δ	Thickness (m)
ω	Humidity ratio (kg/kg)

Subscript

a	Air
d	Desiccant
HX	Heat exchanger
HTF	Heat transfer fluid
avg	Averaged
in	Inlet air
out	Outlet air
r	Regeneration
p	Process
ref	Reference
sat	saturation
lam	Laminar
tur	Turbulent
q	Isoflux
T	Isothermal

section 2.1 for working principles, can significantly reduce the electricity consumption [11,12]. Recently, desiccant coated heat exchangers (DC-HXs), which are manufactured by coating with a desiccant material on a heat exchanger (e.g. fin-tube), has received immense attention due to its advantages, namely reducing the energy consumption and efficient dehumidification performance. Heat and moisture transfer are highly coupled in DC-HX during regeneration and dehumidification processes. This makes it difficult to handle both latent and sensible loads by only using DC-HX. In order to provide comfortable air temperature and humidity levels (Temperature of 20–24 °C and RH of 30–60 % [13]), sensible and latent loads of the process air can be handled separately by adding an extra system for handling the sensible load, e.g. an evaporative cooling system [14].

Several studies have been conducted to investigate the characteristics of DC-HX. Amani et al. [15] studied the effects of operating parameters on the performance of a new FAM-Z02 DC-HX for greenhouse applications. They reported cyclic moisture removal capacity (MRC) and dehumidification coefficient of performance (DCOP) in the range of 2.5–4.0 and 0.18–0.3, defined in Eqs.(19) and (21), thereby introducing suitable performance for greenhouse conditions. Ge et al. [16,17] proposed a numerical model and studied the effects of main operation parameters and climatic conditions. Their model assumed that there was only heat and mass transfer in one direction in a DC-HX. The accuracy of their model was validated over a range of operation conditions, with a relative difference of ± 15 %. Saeed and Al-Alili [18] summarized the empirical and numerical studies implemented on DC-HXs and reported that SAPO34 generally has better dehumidification performance compared to FAPO34 and silica gel. Zhao et al. [19] investigated a silica gel-based DC-HX experimentally and reported that the DC-HX system efficiency is affected remarkably by cycle time. Sun et al. [20] considered DC-HX with different structure sizes and concluded that the unit with the highest surface compactness (the ratio of the total transfer surface area to the total volume of the exchanger) has the greatest heat and mass transfer performance, while higher air pressure drop was a penalty. Erkek et al. [21] simulated a small-scale adiabatic and liquid-cooled DC-HX using Modelica modeling language [22]. Their results showed the advantages of a liquid-cooled dehumidification system over adiabatic ones. Jagirdar and Lee [23] simulated heat and mass exchange phenomena of a DC-HX using a finite volume method. They considered fin efficiency as well as solid side mass transfer resistance in their modeling and concluded that DC-HX has the potential to replace conventional AC units if low-grade heat (50 °C) is available. Vivekh et al. [24] developed a computational fluid dynamic approach to simulate the simultaneous heat and mass transfer phenomena in DC-HX. The maximum discrepancy between the modeling and experimental results were reported to be ± 14 %.

There are only a few studies in the literature that introduced analytical solution for sorption-based heat exchangers. Lee and Kim [25] simplified the governing equations of a desiccant wheel to a set of linear ordinary differential equations using an integral model. Kang et al. [26,27] used an explicit analytic solution for heat/mass transfer in a desiccant wheel assuming linearized humidity and temperature profiles and the root mean square errors of less than 10 % were reported. Bahrehmand et al. [28,29] proposed a novel analytical model to study the performance of coated sorption beds and oscillatory heat transfer in air conditioning units, for sorption closed-cycle, i.e. where non-condensable gases (NCG), e.g. air, were not present. Although not directly applicable to DC-HX dehumidification systems– which can be categorized as open-cycle sorption system since NCG are present– their analytical approach is quite relevant and noteworthy. They employed orthogonal expansion technique to solve the transient 2-D equations and validated their results with measurements. In another study, Bahrehmand and Bahrami [30] introduced an analytical design tool for sorber bed heat exchangers, and reported that the cycle time, sorption composite composition, heat transfer characteristics, and sorber bed geometry can have conflicting counter effects on the performance, therefore should be optimized simultaneously.

To the best of authors' knowledge, the approach of majority of studies associated with DC-HXs is numerical and experimental analyses and there is no analytical model that can accurately predict the heat and moisture transfer in a DC-HX in the literature. Due to the complicated nature of DC-HX, solving the highly-coupled transient heat and mass transfer equations using numerical simulations are rather time-consuming and as a result may be impractical for real-time system optimization and seasonal simulations. Thus, the gap of research is felt. Therefore, the objective of this study is to develop a new closed-form analytical solution to evaluate the performance of DC-HX. In the present analytical model, both linear and exponential profiles are examined for the air temperature and humidity ratio along the heat/mass exchanger and the results are compared to the experimental data. To validate the proposed model, an AQSOA™-FAM-Z02 DC-HX is built and tested over a range of operating conditions in a custom-built testbed in

our lab.

2. DC-HX principle of operation and the experimental setup

2.1. DC-HX working principle

Fig. 1(a) shows a sorption coated on the fins of a fin-tube heat exchanger. In the DC-HX, the process air flows over the fins of the exchanger and is dehumidified. During the adsorption process, a cooling heat transfer fluid (HTF) is circulated in the exchanger to remove the generated adsorption heat, thereby enhancing the dehumidification efficiency. The desiccant becomes saturated at the end of the dehumidification process. In the regeneration process, hot HTF is circulated through the exchanger to evaporate the water vapor from the desiccant (regenerate the active material). A schematic view of the working principle of a DC-HX is shown in Fig. 1(b).

2.2. Experimental setup

In order to verify our analytical solution, an AQSOA™-FAM-Z02 DC-HX was built and tested. AQSOA™-FAM-Z02 was introduced for air-conditioning applications by Mitsubishi Chemical Ltd. [33]. Isotherm of FAM-Z02 has been measured in our lab and depicted in Fig. 2.

Our custom-built testbed is shown in Fig. 3. The testbed consisted of an environmental chamber, a fan, a duct, a voltage regulator, a data acquisition system, and two thermostatic baths. The environmental chamber which simulated the indoor air condition supplied the air using a centrifugal fan. The air flow rate is adjusted by a voltage regulator. The

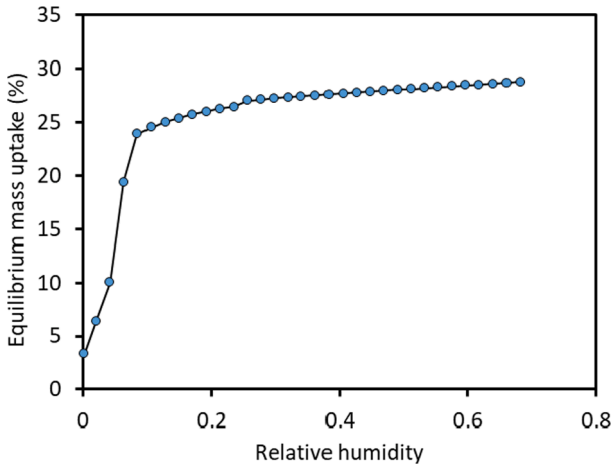

Fig. 2. Isotherm curve of AQSOA FAM-Z02 DC-HX at 20 °C.

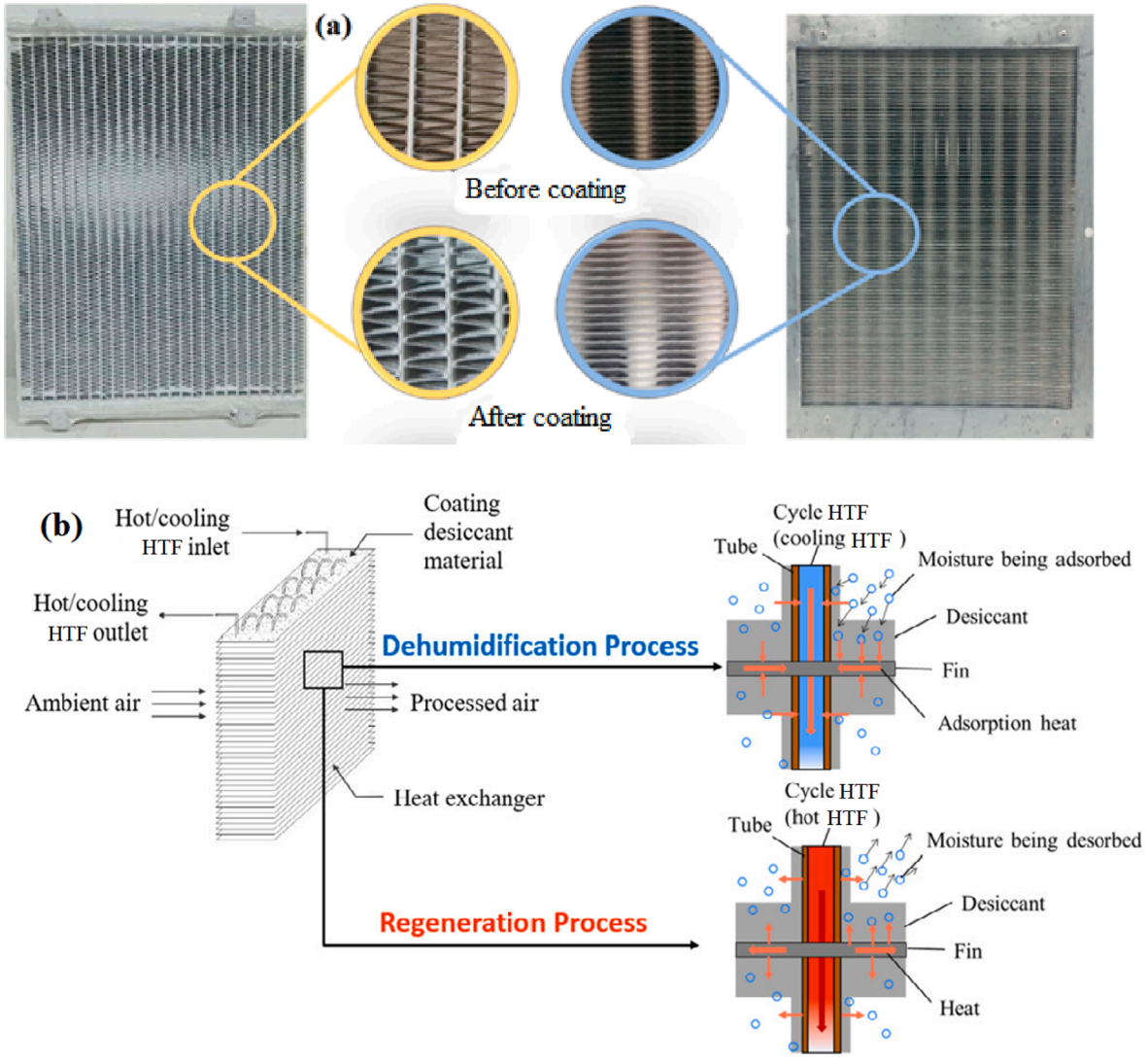

Fig. 1. (a) Image of a DC-HX [31]; (b) working principle of DC-HX [32].

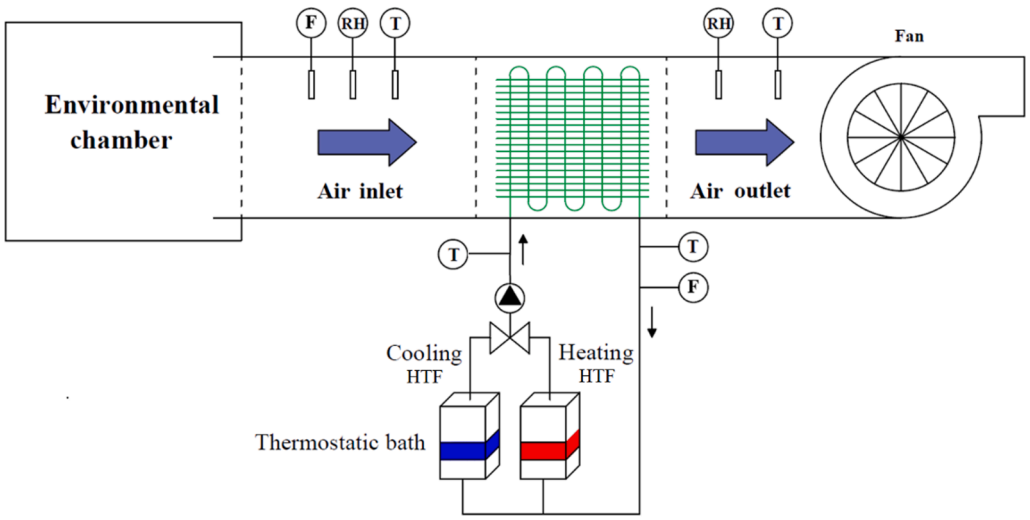

(a)

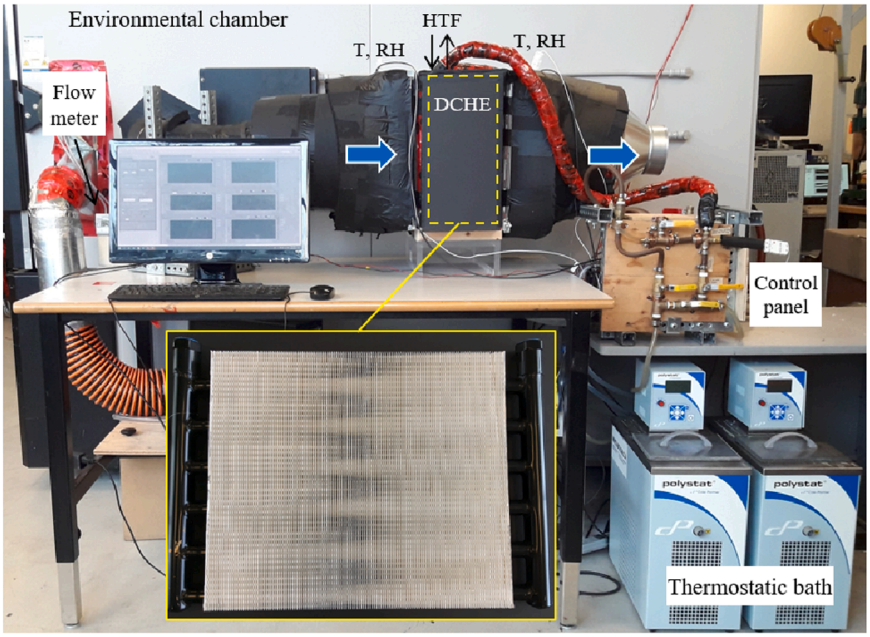

(b)

Fig. 3. (a) Schematic diagram (b) a photo of the custom-built testbed in our lab.

air and HTF temperature and air RH at the inlet and outlet of the heat/mass exchanger were measured using PT100 and Vaisala-HMP110 sensors with the accuracy of ± 0.1 °C and ± 1.5 %RH, respectively. To measure the airflow rate, an orifice plate (4″ Oripac© model 4150) with the accuracy of ± 0.25 % of the measured value was employed. Two Polystat® cooling/heating thermostatic baths were used to attain desired cooling and hot HTF temperatures. Finally, the data were collected using LABVIEW software [34] with a sampling interval of 3 s. The details of the DC-HX in our study is presented Table 1.

The operating conditions of the experimental analysis are listed in Table 2. The analytical solution validation conditions can be found in the third column of Table 2.

Table 1
Specifications of the DC-HX.

Parameter	Value
Heat exchanger dimension	305 × 355 × 38 (mm)
Mass of heat exchanger	7250 (g)
Fin pitch	2.3 (mm)
Fin thickness	0.1 (mm)
Tube diameter	8.25 (mm)
Tube material	Copper
Fin material	Aluminum
Desiccant weight	800 (g)
Desiccant thickness	0.3 (mm)

Table 2
Operating conditions of the experiments.

Parameters	Experimental conditions	Validation conditions
Airflow rate	34–136 m^3/hr	34 and 136 m^3/hr
Air temperature	10–30 °C	20 °C
Air relative humidity	40–90 %	60 %
Cooling HTF temperature	5–30 °C	10 °C
Hot HTF temperature	50–90 °C	70 °C

2.3. Uncertainty analysis

The method proposed by Kline and McClintock [35] is used to calculate the uncertainty of the experimental study as follow:

$$\Delta y = \left[\left(\frac{\partial f}{\partial x_1}\Delta x_1\right)^2 + \left(\frac{\partial f}{\partial x_2}\Delta x_2\right)^2 \cdots + \left(\frac{\partial f}{\partial x_n}\Delta x_n\right)^2\right]^{\frac{1}{2}} \quad (1)$$

$$\frac{\Delta y}{y} = \left[\left(\frac{\partial f}{\partial x_1}\frac{\Delta x_1}{y}\right)^2 + \left(\frac{\partial f}{\partial x_2}\frac{\Delta x_2}{y}\right)^2 \cdots + \left(\frac{\partial f}{\partial x_n}\frac{\Delta x_n}{y}\right)^2\right]^{\frac{1}{2}} \quad (2)$$

where, x_1, x_2 etc. are the independent variables of f function, Δx_1, Δx_2 etc. denote the absolute error of variables and $\Delta y/y$ represents the relative error. Based on this method, calculated uncertainties of measured MRC and DCOP are 8.4 % and 10.3 %, respectively.

3. Analytical model

A simplified 2-D geometry is considered and shown schematically in Fig. 4. This geometry consisted of air stream, desiccant layer, heat exchanger (HX), and HTF. Based on the physics of adsorption/desorption cycles, cyclic steady state is assumed for the presented model. The following additional assumptions are made to simplify the model development:

Thermophysical properties for the air, HX, and desiccant layer are assumed constant.

The regeneration temperature is low (less than 90 °C [36]). Thus, a constant enthalpy of adsorption (h_{ad}) is assumed following Ref. [37].

Air stream is assumed to be fully-developed over the heat/mass exchanger. Therefore, the heat and mass transfer coefficients are considered constant over time.

Axial heat conduction in the air stream and desiccant layer are considered negligible.

Lewis number equal to unity is assumed.

Constant average values are considered for the rate of change in the water uptake (W_d) with respect to humidity ratio and the desiccant layer temperature ($\frac{\partial W_d}{\partial \omega_d}$ & $\frac{\partial W_d}{\partial T_d}$). This assumption is justified when humidity ratio and temperature do not change significantly during a cycle [26].

The effects of unsteady terms in the air stream ($\frac{\partial T_a}{\partial t} \approx \frac{\partial \omega_a}{\partial t} \approx 0$) are assumed negligible, following Ref. [26].

HTF temperature along the channel is assumed to remain constant; this assumption is in agreement with our measurements.

As the desiccant layer is thin, averaged properties in the y-direction are used, namely, $T_d(x,t), \omega_d(x,t)$ [38].

Convective effects of the sorbate inside the sorbent coating are negligible as the coating is thin and the vapor pressure is fairly low [26,28,29,39,40].

Sorption/desorption heat is released/absorbed at the interface between the desiccant layer and the air.

Based on well-stablished internal flow studies, air temperature and humidity profiles are assumed to be exponential in the x-direction (See Eq.(4)) [41]. Previous studies assumed linear change in the x-direction (Eq.(3)) for the air temperature and humidity profiles [26,27]. This assumption is valid for high flow rates and short channels and will be discussed further in the present study. In this study, both linear and exponential assumptions are assumed and compared with experimental data.

3.1. Governing equations

As shown in Fig. 4, two control volumes CV_1 and CV_2 are considered, where the energy and mass exchanges between: i) the air with desiccant layer (CV_1); and ii) the desiccant layer and HX with HTF and air (CV_2). Based on the above-mentioned assumptions, the energy and mass balances for each control volume are expressed as:

Energy and mass balance in CV_1.

$$u_{avg}\frac{\partial T_a(x,t)}{\partial x} = \frac{1}{\rho_a c_{P,a} H} h(T_d(x,t) - T_a(x,t)) \quad (1)$$

$$u_{avg}\frac{\partial \omega_a(x,t)}{\partial x} = \frac{1}{H} h_m(\omega_d(x,t) - \omega_a(x,t)) \quad (2)$$

where, u_{avg}, $T_a(x,t)$ and $\omega_a(x,t)$ are average values in y-direction for air velocity, temperature and humidity ratio, respectively. The average temperature of air as listed in the assumptions is calculated based on two different profiles as:

In which $a(t)$ is an unknown function of time, which should be

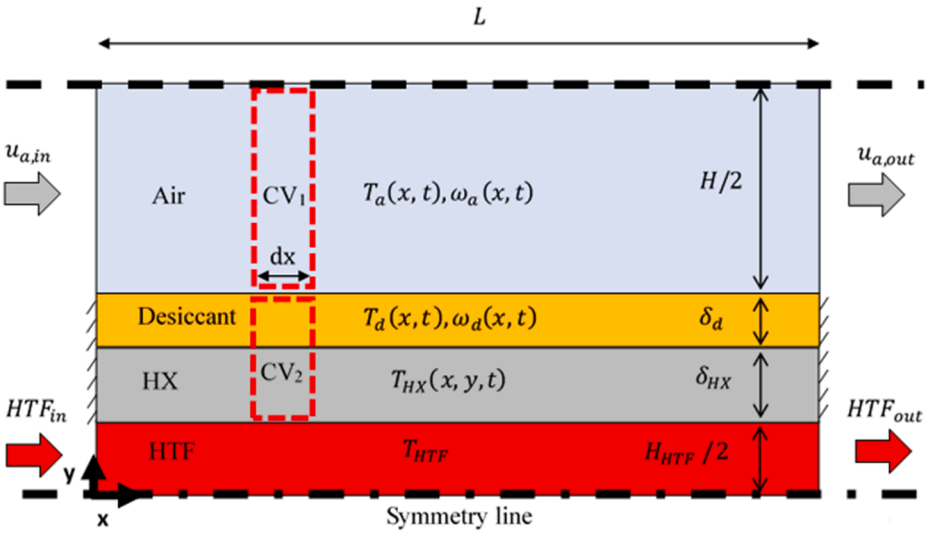

Fig. 4. Sectional schematic view of DC-HX calculation domain and selected control volumes for the present model.

calculated and S_1 is listed in Table 4.

Energy and mass balance in CV_2.

$$\rho_d c_{P,d}\delta_d\frac{\partial T_d(x,t)}{\partial t}+\rho_{HX}c_{P,HX}\delta_{HX}\frac{\partial T_{HX,avg(in\,y)}(x,t)}{\partial t}=h_{ad}\rho_a h_m(\omega_a(x,t)-\omega_d(x,t))+h(T_a(x,t)-T_d(x,t))+h_{HTF}(T_{HTF}-T_{HX}(x,H_{HTF}/2,t))+k_{HX}\delta_{HX}\frac{\partial^2 T_{HX,avg(in\,y)}(x,t)}{\partial x^2} \tag{5}$$

$$\frac{\partial W_d(x,t)}{\partial T_d(x,t)}\frac{\partial T_d(x,t)}{\partial t}+\frac{\partial W_d(x,t)}{\partial \omega_d(x,t)}\frac{\partial \omega_d(x,t)}{\partial t}=\frac{\rho_a}{\rho_d\delta_d}h_m(\omega_a(x,t)-\omega_d(x,t)) \tag{6}$$

The governing equations should be solved simultaneously with the following initial conditions. These conditions are derived based on cyclic steady state assumption and the fact that there is no temperature or humidity ratio jump in the desiccant layer while switching from adsorption to regeneration and vice versa:

$$\begin{cases}\omega_d(x,0)=\omega_d(x,t_r+t_p)At\ \ the\ \ beginning\ \ of\ \ regeneration\\ \omega_d(x,t_r-\varepsilon)=\omega_d(x,t_r+\varepsilon)At\ \ the\ \ beginning\ \ of\ \ process\\ T_d(x,0)=T_d(x,t_r+t_p)At\ \ the\ \ beginning\ \ of\ \ regeneration\\ T_d(x,t_r-\varepsilon)=T_d(x,t_r+\varepsilon)At\ \ the\ \ beginning\ \ of\ \ process\end{cases} \tag{7}$$

In which t_p and t_r are process and regeneration time, ε is an infinite small time step, $t_r-\varepsilon$ and $t_r+\varepsilon$ represent the end of regeneration process and beginning of the adsorption, respectively. The derivation method of parameters used in the above governing equations are summarized in Table 3.

To develop a generalized solution for various conditions and geometries, proper dimensionless parameters should be defined, which are listed in Table 4.

By averaging the above equations over the length of the DC-HX (axial direction) ($\frac{1}{L}*\int_0^L dx$) and introducing the dimensionless variables listed in Table 4, the following equations are obtained.

- Energy balance in CV_1

$$\left(\theta_{a,out,p}(\tau)-\theta_{a,in,p}\right)=S_1\left(\theta_{d,avg}(\tau)-\theta_{a,avg,p}(\tau)\right) \tag{8}$$

$$\left(\theta_{a,out,r}(\tau)-\theta_{a,in,r}\right)=S_1\left(\theta_{d,avg}(\tau)-\theta_{a,avg,r}(\tau)\right) \tag{9}$$

- Mass balance in CV_1

$$\left(\Omega_{a,out,p}(\tau)-\Omega_{a,in,p}\right)=S_1\left(\Omega_{d,avg,p}(\tau)-\Omega_{a,avg,p}(\tau)\right) \tag{10}$$

$$\left(\Omega_{a,out,r}(\tau)-\Omega_{a,in,r}\right)=S_1\left(\Omega_{d,avg,r}(\tau)-\Omega_{a,avg,r}(\tau)\right) \tag{11}$$

- Energy balance in CV_2

$$\frac{\partial\theta_{d,avg,p}(\tau)}{\partial\tau_p}=\left[S_{2,p}\left(\Omega_{a,avg,p}(\tau)-\Omega_{d,avg,p}(\tau)\right)+S_{3,p}\left(\theta_{a,avg,p}(\tau)-\theta_{d,avg,p}(\tau)\right)-S_{4,p}\left(\theta_{d,avg,p}(\tau)-\theta_{HTF,p}\right)\right] \tag{12}$$

$$\frac{\partial\theta_{d,avg,r}(\tau)}{\partial\tau_r}=\left[S_{2,r}\left(\Omega_{a,avg,r}(\tau)-\Omega_{d,avg,r}(\tau)\right)+S_{3,r}\left(\theta_{a,avg,r}(\tau)-\theta_{d,avg,r}(\tau)\right)-S_{4,r}\left(\theta_{d,avg,r}(\tau)-\theta_{HTF,r}\right)\right] \tag{13}$$

- Mass balance in CV_2

$$S_{\theta,p}\frac{\partial\theta_{d,avg,p}(\tau)}{\partial\tau_p}+S_{\Omega,p}\frac{\partial\Omega_{d,avg,p}(\tau)}{\partial\tau_p}=S_{5,p}\left(\Omega_{a,avg,p}(\tau)-\Omega_{d,avg,p}(\tau)\right) \tag{14}$$

$$S_{\theta,r}\frac{\partial\theta_{d,avg,r}(\tau)}{\partial\tau_r}+S_{\Omega,r}\frac{\partial\Omega_{d,avg,r}(\tau)}{\partial\tau_r}=S_{5,r}\left(\Omega_{a,avg,r}(\tau)-\Omega_{d,avg,r}(\tau)\right) \tag{15}$$

The above system of equations needs four initial values. As it was mentioned, considering the cyclic nature of the DC-HX operation, four initial conditions for $\Omega_{d,avg,p}$, $\Omega_{d,avg,r}$, $\theta_{d,avg,p}$, and $\theta_{d,avg,r}$ could be obtained as follows:

$$\begin{cases}\Omega_{d,avg,p}(0)=\Omega_{d,avg,r}(1)At\ \ the\ \ beginning\ \ of\ \ process\\ \Omega_{d,avg,r}(0)=\Omega_{d,avg,p}(1)At\ \ the\ \ beginning\ \ of\ \ regeneration\\ \theta_{d,avg,p}(0)=\theta_{d,avg,r}(1)At\ \ the\ \ beginning\ \ of\ \ process\\ \theta_{d,avg,r}(0)=\theta_{d,avg,p}(1)At\ \ the\ \ beginning\ \ of\ \ regeneration\end{cases} \tag{16}$$

A general form of the final solution for the dimensionless desiccant

Table 3
Derivation of used parameters in the governing equations.

Parameter	Formula
ω	$0.622RHP_{sat}/(P_{atm}-RHP_{sat})$ [42]
$Nu_{q,lam}$(isoflux)	4.36 [41]
$Nu_{T,lam}$(isothermal)	3.66 [41]
$Nu_{avg,lam}$	$(Nu_{T,lam}+Nu_{q,lam})/2$
h	$Nu_{avg,lam}k_a/H$
h_m	$h/\rho c_p$ [41]
Nu_{tur}	$0.023Re^{4/5}\,\mathrm{Pr}^{1/3}$ [41]
h_{HTF}	$Nu_{tur}k_{HTF}/H_{HTF}$

Table 4
Definition of the dimensionless variables used in the analytical solution.

Dimensionless time	$\tau_r=\frac{t}{t_r}$, $\tau_p=\frac{t}{t_p}$
Dimensionless temperature (T_{ref} is an arbitrary value; not equal to T_p)	$\theta=\frac{T-T_p}{T_{ref}-T_p}=\frac{T-T_p}{\Delta T}$
Dimensionless humidity ratio (ω_{ref} is an arbitrary value; not equal to ω_p)	$\Omega=\frac{\omega-\omega_p}{\omega_p-\omega_{ref}}=\frac{\omega-\omega_p}{\Delta\omega}$
Rate of change in uptake with dimensionless temperature	$S_\theta=\frac{\partial W_d(\tau)}{\partial\theta_{d,avg}(\tau)}$
Rate of change in uptake with dimensionless humidity ratio	$S_\Omega=\frac{\partial W_{d,avg}(\tau)}{\partial\Omega_{d,avg}(\tau)}$
Convection heat/mass transfer rate in air over heat/mass carried by air mass flow (advection)	$S_1=\frac{hL}{u_{avg}\rho_a c_{P,a}H}=\frac{h_m L}{u_{avg}H}$
Adsorption heat generation over heat stored in HX and desiccant layer	$S_{2,p\,(or\,r)}=\frac{h_{ad}\rho_a h_m\Delta\omega\, t_{p\,(or\,r)}}{(\rho_d c_{P,d}\delta_d+\rho_{HX}c_{P,HX}\delta_{HX})\Delta T}$
Amount of heat transferred from desiccant to air over thermal inertia of HX and desiccant layer	$S_{3,p\,(or\,r)}=\frac{h\,t_{p\,(or\,r)}}{(\rho_d c_{P,d}\delta_d+\rho_{HX}c_{P,HX}\delta_{HX})}$
Amount of heat transferred from HX to HTF over thermal inertia of HX and desiccant layer	$S_{4,p\,(or\,r)}=\frac{h_{HTF}\,t_{p\,(or\,r)}}{(\rho_d c_{P,d}\delta_d+\rho_{HX}c_{P,HX}\delta_{HX})}$
Convection mass transfer over mass of desiccant layer	$S_{5,p\,(or\,r)}=\frac{\rho_a h_m t_{p\,(or\,r)}}{\rho_d\delta_d}$

Table 5
List of constants in the final solution of outlet air temperature.

$$B_{i,j} = \frac{A\,S_{2,j}\left(\Omega_{a,in,j'} - \Omega_{a,in,j}\right) - \left(\frac{X_{3,j'}}{X_{2,j'}} - \frac{X_{3,j}}{X_{2,j}}\right)\left[S_1\lambda_{i',j} - \left(AS_{3,j} + S_1S_{4,j}\right)\right]}{S_1\left(\lambda_{i,j} - \lambda_{i',j}\right)}$$

$$\lambda_{i,j} = \left(X_{1,j} \pm \sqrt{X_{1,j}^2 - 4X_{2,j}}\right)\Big/2$$

$$A = \begin{cases} (1 - exp(-S_1)) \text{ for linear profile} \\ \dfrac{2S_1}{S_1 + 2} \text{ for exponential profile} \end{cases}$$

$$X_{1,j} = \left(-\frac{S_\theta}{S_{5,j}} + \frac{S_{3,j}S_\Omega}{S_{2,j}S_{5,j}} + \frac{S_1S_{4,j}S_\Omega}{AS_{2,j}S_{5,j}} + \frac{\Delta\omega}{S_{2,j}}\right) \times \frac{AS_{2,j}S_{5,j}}{S_1S_\Omega}$$

$$X_{2,j} = \left(\frac{AS_{3,j}\Delta\omega}{S_1S_{2,j}} + \frac{S_{4,j}\Delta\omega}{S_{2,j}}\right) \times \frac{AS_{2,j}S_{5,j}}{S_1S_\Omega}$$

$$X_{3,j} = \left(\frac{AS_{3,j}\Delta\omega}{S_1S_{2,j}}\theta_{a,in,j} + \frac{S_{4,j}\Delta\omega}{S_{2,j}}\theta_{HTF}\right) \times \frac{AS_{2,j}S_{5,j}}{S_1S_\Omega}$$

$$i = 1 \text{ or } 2 \Rightarrow i' = \begin{cases} 2 \text{ if } i = 1 \\ 1 \text{ if } i = 2 \end{cases} \quad j = p \text{ or } r \Rightarrow j' = \begin{cases} r \text{ if } j = p \\ p \text{ if } j = r \end{cases}$$

temperature and outlet air temperature for adsorption process, are shown in Eq.(17) and Eq.(18), respectively and the constants are listed in Table 5. The details of the solution for both heat and mass transfer during adsorption and regeneration can be found in Appendix A: Solution detail.

$$\theta_{d,avg,p}(\tau) = B_{1,p}exp(-\lambda_{1,p}\tau) + B_{2,p}exp(-\lambda_{2,p}\tau) + X_{3,p}/X_{2,p} \tag{17}$$

$$\theta_{a,out,p}(\tau) = A\,\theta_{d,avg,p}(\tau) + (1 - A)\theta_{a,in,p} \tag{18}$$

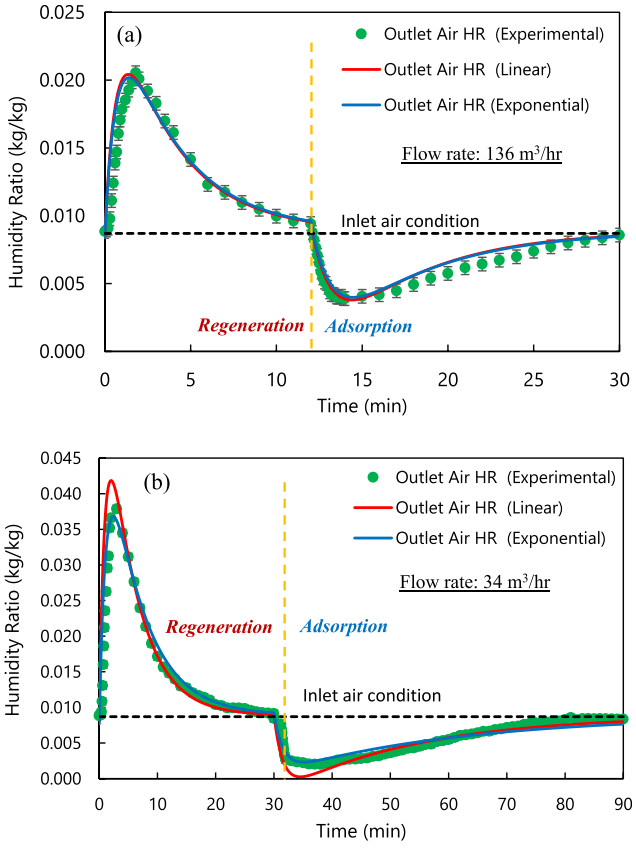

Fig. 5. Comparison between the present models, assuming both linear and exponential profiles for temperature and humidity ratio, against collected data (±0.5 gr/kg uncertainty) collected in our lab. Variation of outlet air humidity ratio for air flow rate of (a) 136 and (b) 34 m^3/hr.

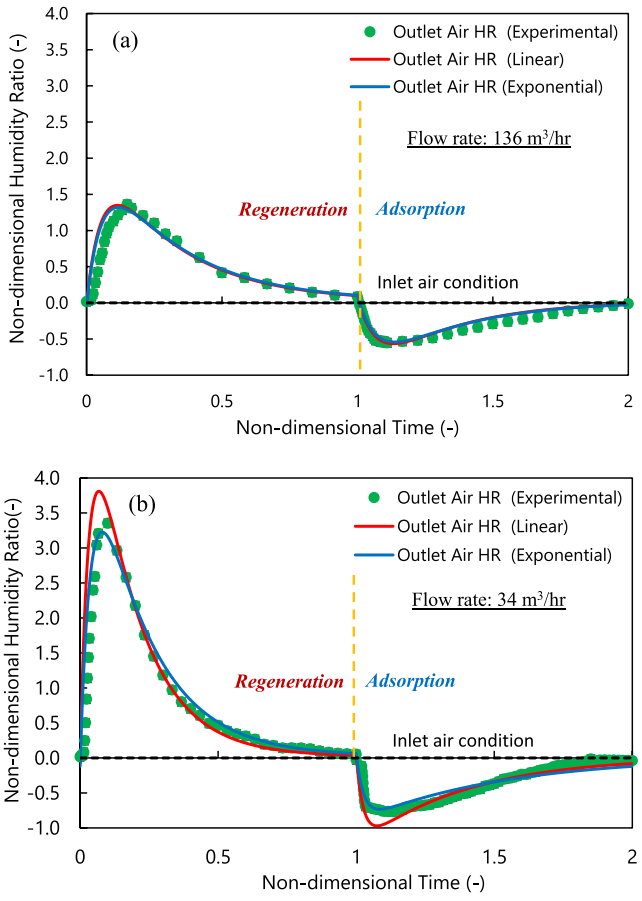

Fig. 6. Comparison between the present models, assuming both linear and exponential profiles for temperature and humidity ratio, against collected data (±0.06 (-) uncertainty) collected in our lab in non-dimensional form. Variation of non-dimensional outlet air humidity ratio ($\Omega = \frac{\omega - \omega_p}{\omega_p - \omega_{ref}}$) for air flow rate of (a) 136 and (b) 34 m3/hr.

3.2. Performance indices

To evaluate the performance of the DC-HX, the commonly-used moisture removal capacity (MRC) and dehumidification coefficient of performance (DCOP) parameters are used in this study. The time-averaged moisture removal during the adsorption process, MRC, can be calculated as follows [43]:

$$MRC = \frac{3600*1000}{t_p + t_r}\int_0^{t_r} \dot{m}_a\left(\omega_{a,out} - \omega_{a,in}\right)dt \tag{19}$$

which can also be described based on the simplified non-dimensional solution as:

$$MRC = -3.6 \times 10^6 \frac{t_r}{t_p + t_r}\rho u H\,\Delta\omega \int_0^1 \left(\Omega_{a,out,r} - \Omega_{a,in,r}\right)d\tau$$

$$= 3.6 \times 10^6 \frac{t_r}{t_p + t_r}\frac{\rho u H \Delta\omega}{AS_{2,r}}\left[\left(\frac{B_{1,r}}{\lambda_{1,r}} + \frac{B_{2,r}}{\lambda_{2,r}}\right)\left(AS_{3,r} + S_1S_{4,r}\right) + S_1\left(B_{2,r} + B_{1,r}\right)\right] \tag{20}$$

It should be noted that to calculate the amount of water which is adsorbed/desorbed during one cycle, MRC should be multiplied by cycle time ($t_p + t_r$).

DCOP is the ratio of the latent heat removed during the adsorption process ($\dot{Q}_{lat}$) over the heat exchanged of HTF during the regeneration process ($\dot{Q}_{reg}$). The electrical power input of the pumps and fans are

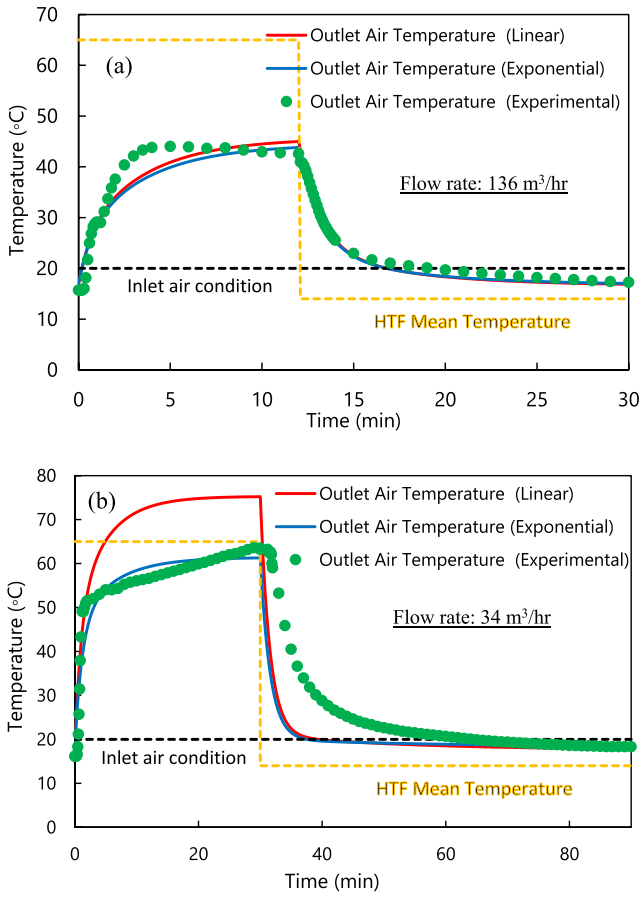

Fig. 7. Comparison between the present models (linear & exponential) against collected data (±0.1 °C uncertainty). Variation of outlet air temperature for air flow rate of (a) 136 and (b) 34 m^3/hr.

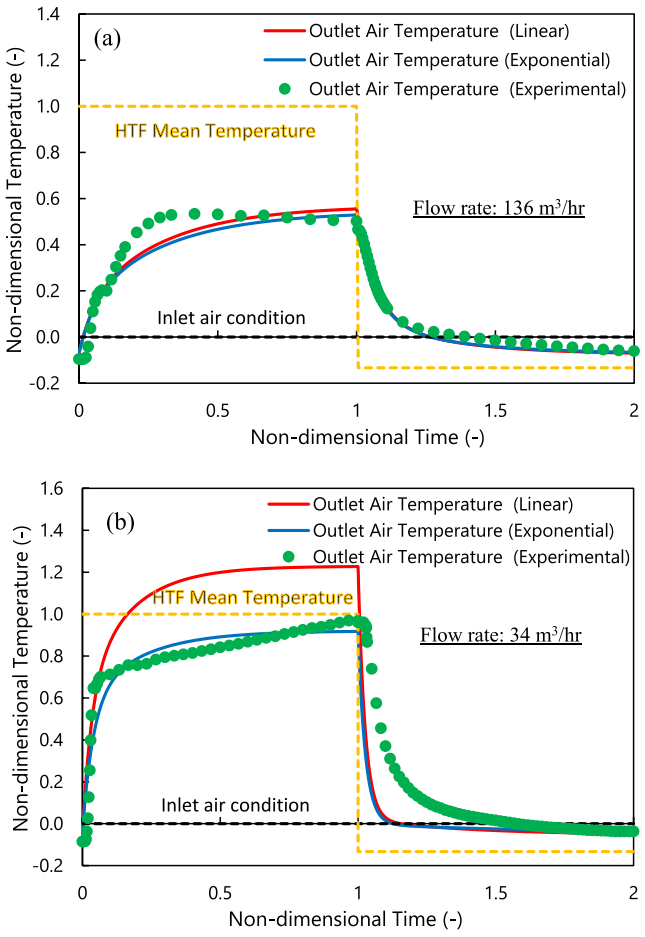

Fig. 8. Comparison between the present models (linear & exponential) against collected data (±0.002 (-) uncertainty) in non-dimensional form. Variation of non-dimensional outlet air temperature ($\theta = \frac{T-T_p}{T_{ref}-T_p}$) for air flow rate of (a) 136 and (b) 34 m3/hr.

rather small and neglected. The DCOP can be computed using the following equation [44]:

$$DCOP = \frac{\dot{Q}_{lat}}{\dot{Q}_{reg}} = \frac{\dot{m}_a(\omega_{a,in} - \omega_{a,out})h_{ads}}{\dot{m}_w c_{pw}(T_{w,in} - T_{w,out})} \tag{21}$$

which can also be described based on the non-dimensional solution as:

$$DCOP = \frac{1}{A\,S_1 S_{4,r}} \frac{\left(\frac{B_{1,r}}{\lambda_{1,\,r}} + \frac{B_{2,r}}{\lambda_{2,\,r}}\right)\left(AS_{3,r} + S_1 S_{4,r}\right) + S_1\left(B_{2,r} + B_{1,\,r}\right)}{\theta_{HTF,r} - \left(\frac{B_{1,r}}{\lambda_{1,r}} + \frac{B_{2,r}}{\lambda_{2,r}} + \frac{X_{3,r}}{X_{2,r}}\right)} \tag{22}$$

4. Results and discussion

In this study, both linear and exponential profiles are considered for the air temperature and humidity ratio along the DC-HX. For model validation, the present analytical solution is compared to the experimental data collected in our lab, see Table 1 for the details of the developed and tested DC-HX in this study. Fig. 5 (Fig. 6 in non-dimensional form) shows the variation of the outlet air humidity ratio for air flow rate of 34 and 136 m^3/hr. During regeneration or adsorption process, the area between the outlet (blue or red line) and inlet (black dashed line) air HR curves (Fig. 5), represents the amount of water desorbed/adsorbed in one cycle, i.e., MRC (See Eq.(19)). It should be noted that based on the cyclic steady state nature of the system, calculated areas for both regeneration and adsorption process are identical. However, in non-dimensional form (Fig. 6), because of the difference in regeneration and adsorption process time, these two areas are not identical and do not represent MRC. To have a representation of MRC based on the non-dimensional curves, each of the areas should be multiplied by their actual duration (t_r and t_p). (See Eq.(20)).

As can be seen from Fig. 5(a), the proposed analytical solution predicts the experimental data accurately for both linear and exponential profile assumptions for air flow rate of 136 m^3/hr, with an averaged relative difference of 5 %. Fig. 5(b) indicates that the exponential profile for the air temperature and humidity ratio provides a slightly better agreement with our experimental results with an averaged relative difference of 10 %, while linear profile assumption overestimates the outlet humidity ratio at the peaks.

Fig. 7. (Fig. 8 in non-dimensional form) shows the variation of outlet air temperature for air flow rate of 34 and 136 m^3/hr. It should be noted that the area between the outlet (blue or red line) and inlet (black dashed line) air temperature curves (Fig. 7) represent the sensible heat transferred to and removed from air during the desorption/adsorption process. As shown in Fig. 7(a), the present analytical solution predicts the experimental data accurately for both linear and exponential profile assumptions for the air flow rate of 136 m^3/hr, with relative difference of 5 %. Fig. 7(b) reveals that considering the exponential profile for the air velocity has a good agreement with the experimental results, with relative difference of 10 %, while linear profile assumption leads to unrealistic results.

The relative difference between the two assumed profiles are also calculated for temperature and humidity ratio with maximum values of 30 %, 20 % and average values of 10 % and 5 %, respectively.

The linear velocity assumption is perhaps not valid for high C_1 =

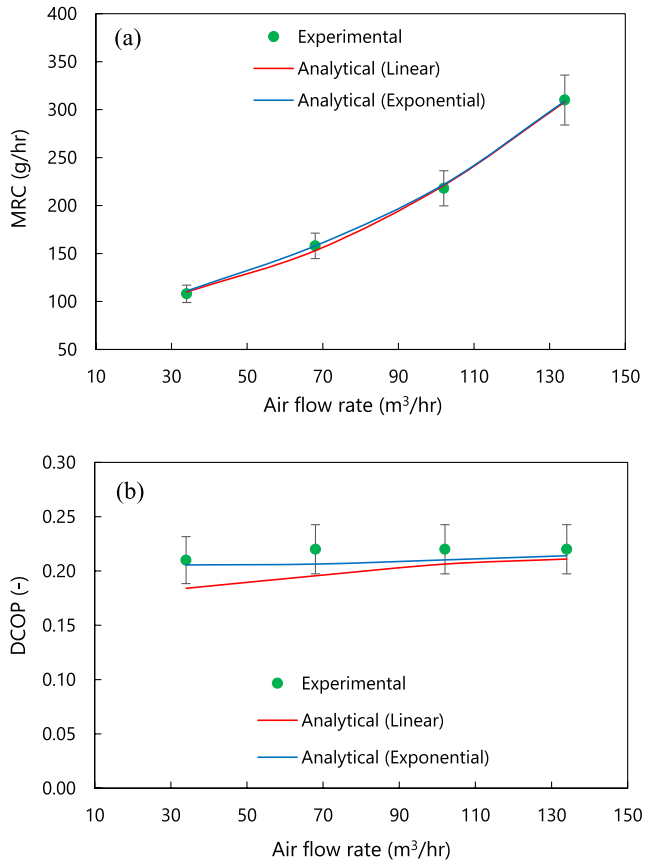

Fig. 9. Comparison of the pre sen t models (linear & exponential) against collected data for (a) MRC and (b) DCOP vs air flow rate.

$\frac{hL}{u\rho_a c_{p,a} H}$ (see Table 4) values. This can be explained by considering that when C_1 is high, the heat/mass transferred to air is relatively high, thereby leading to a significant change in air temperature/humidity ratio profile at the entrance of the air channel in the DC-HX. This can cause an error in a linear assumption. On the other hand, exponential profile is capable to take this rather fast change into account and shows more accurate results even for high C_1 values.

The MRC and DCOP of the studied DC-HX are also compared for various air flow rates. It should be noted that the regeneration and adsorption cycle time varies for each air flow rate (34–136 m^3/hr). The cycle time is set in a way that at the end of each process, the DC-HX is saturated, i.e., the outlet air approaches a steady-state condition. Fig. 9 (a) shows the MRC change with the air flow rate. As it can be seen, both assumptions show good prediction for MRC. As it was mentioned before, linear assumption's error is mostly in prediction of peak's humidity ratio, which in current experiment is relatively short in comparison with adsorption/desorption time. It means that by choosing shorter adsorption/desorption time this error is more emphasized. Fig. 9(b) shows DCOP change with air flow rate. Exponential assumption shows a good agreement with experimental data. As it is expected, linear assumption error in lower air flow rates increases.

5. Conclusion

A new closed-form analytical model is developed that can predict the performance of a DC-HX and validated against experimental data collected in this study. The present model accurately predicts: i) the humidity ratio, ii) temperature variations, iii) MRC, and iv) DCOP of the DC-HX. Both assumptions of linear and exponential profiles are considered for the air flow temperature and humidity ratio. After careful examination and comparison with experimental data, it is concluded that an exponential profile is more realistic as it provides more accurate results for the DC-HX with average relative difference of than 10 %, compared to linear profile with relative difference of 20 %. This study provides insight in the heat and mass transfer and adsorption processes involved in DC-HX and offer a computationally efficient tool for optimal design and real-time control of dehumidification systems for a wide range of applications.

Declaration of Competing Interest

The authors declare that they have no known competing financial interests or personal relationships that could have appeared to influence the work reported in this paper.

Data availability

No data was used for the research described in the article.

Appendix A:

Solution detail.

To solve the mentioned system of partial differential equations (PDEs) (Eq.(8) to Eq.(15)), following steps were taken:

The results for process (p) and regeneration (r) are shown as following subscript:

$$j = p \; or \; r \Rightarrow j' = \begin{cases} rifj = p \\ pifj = r \end{cases} (e.g.: \theta_{d,avg,j} = 1 \; means: \; \theta_{d,avg,p} = 1 \; \& \; \theta_{d,avg,r} = 1)$$

1- From Eq.(8) and Eq.(9) for both process and regeneration, $\theta_{a,out}(\tau)$ is expressed as functions of $\theta_{a,in}$ and $\theta_{d,avg}(\tau)$. The same expression is obtained for $\Omega_{a,out}$ from Eq.(10) and Eq.(11).

2- Replacing $\Omega_{a,out}$ from step 1 into Eq.(12) and Eq.(13), $\Omega_{d,avg}$ is then obtained based on $\partial\theta_{d,avg}(\tau)/\partial\tau_r$ and $\theta_{d,avg}$.

3- Replacing $\Omega_{d,avg}$ from step 2 into Eq.(14) and Eq.(15), as a result, the two PDEs are turned into second order ordinary differential equations (ODEs):

$$\theta''_{d,avg,j} + X_{1,j}\theta'_{d,avg,j} + X_{2,j}\theta_{d,avg,j} = X_{3,j} \tag{A1}$$

where:

$$\theta'_{d,avg,j} = \partial\theta_{d,avg,j}(\tau)/\partial\tau_r \tag{A2}$$

$$\theta''_{d,avg,j} = \partial^2\theta_{d,avg,j}(\tau)/\partial\tau_r^2 \tag{A3}$$

$$X_{1,j} = \left(-\frac{S_\theta}{S_{5,j}} + \frac{S_{3,j}S_\Omega}{S_{2,j}S_{5,j}} + \frac{S_1 S_{4,j} S_\Omega}{AS_{2,j}S_{5,j}} + \frac{\Delta\omega}{S_{2,j}} \right) \times \frac{AS_{2,j}S_{5,j}}{S_1 S_\Omega} \tag{A4}$$

$$X_{2,j} = \left(\frac{AS_{3,j}\Delta\omega}{S_1 S_{2,j}} + \frac{S_{4,j}\Delta\omega}{S_{2,j}} \right) \times \frac{AS_{2,j}S_{5,j}}{S_1 S_\Omega} \tag{A5}$$

$$X_{3,j} = \left(\frac{AS_{3,j}\Delta\omega}{S_1 S_{2,j}}\theta_{a,in,j} + \frac{S_{4,j)}\Delta\omega}{S_{2,j}}\theta_{HTF} \right) \times \frac{AS_{2,j}S_{5,j}}{S_1 S_\Omega} \tag{A6}$$

For a linear profile assumption, one can use:

$$A = (1 - exp(-S_1)) \tag{A7}$$

For exponential profile assumption, one can use:

$$A = 2S_1/(S_1 + 2) \tag{A8}$$

4- Solving each of the above two ODEs results in a solution with two constants (B_1 and B_2), four in total for adsorption and regeneration air ($B_{1,p(or\,r)}$ and $B_{2,p(or\,r)}$):

As there are two constants, they are shown by the following subscript:

$$i = 1\,or\,2 \Rightarrow i' = \begin{cases} 2 if i = 1 \\ 1 if i = 2 \end{cases} (e.g: B_{i,p} = 1\,means: B_{1,p} = 1\,\&\,B_{2,p} = 1)$$

$$\theta_{d,avg,j}(\tau) = B_{1,j}exp(-\lambda_{1,j}\tau) + B_{2,j}exp(-\lambda_{2,j}\tau) + X_{3,j}/X_{2,j} \tag{A9}$$

where:

$$\lambda_{i,j} = \left(X_{1,j} \pm \sqrt{X_{1,j}^2 - 4X_{2,j}} \right) \Big/ 2 \tag{A10}$$

5- In step 2, $\Omega_{d,avg}$ was obtained based on $\theta_{d,avg}$ and its first derivitive. Following that, an expression for $\Omega_{d,avg}$ with the same constants as $\theta_{d,avg}$ ($B_{1,p(or\,r)}$ and $B_{2,p(or\,r)}$) can be obtained:

$$\Omega_{d,avg,j}(\tau) = \frac{B_{1,j}}{AS_{2,j}}\left(S_1\lambda_{1,j} - \left(AS_{3,j} + S_1 S_{4,j}\right)\right)exp(-\lambda_{1,j}\tau) + \frac{B_{2,j}}{AS_{2,j}}\left(S_1\lambda_{2,\,j} - \left(AS_{3,j} + S_1 S_{4,j}\right)\right)exp(-\lambda_{2,j}\tau) + \Omega_{a,in,j} \tag{A11}$$

6- Applying the initial conditions (Eq.(16)) on Eq. (A9) and Eq.(A11) will lead to the following system of four linear equations and four unknowns, i.e., $B_{1,p(or\,r)}$ and $B_{2,p(or\,r)}$.

Note: $B_{1,p(or\,r)}$ and $B_{2,p(or\,r)}$ equations are found by solving this system of equations. As it is a tedious process, only simplified solution is included here.

$$\theta_{d,avg,p}(0) = \theta_{d,avg,r}(1) \tag{A12}$$

$$\theta_{d,avg,p}(1) = \theta_{d,avg,r}(0) \tag{A13}$$

$$\Omega_{d,avg,p}(0) = \Omega_{d,avg,r}(1) \tag{A14}$$

$$\Omega_{d,avg,p}(1) = \Omega_{d,avg,r}(0) \tag{A15}$$

Based on the fact that heat and mass transfer reach the steady state at the end of each process, it can be concluded that $exp(-\lambda_{i,j})$ is negligible. With this simplification it can be concluded that:

$$B_{i,j} = \frac{A\,S_{2,j}\left(\Omega_{a,in,j'} - \Omega_{a,in,j}\right) - \left(\frac{X_{3,j'}}{X_{2,j'}} - \frac{X_{3,j}}{X_{2,j}}\right)\left[S_1\lambda_{i',j} - \left(AS_{3,j} + S_1 S_{4,j}\right)\right]}{S_1(\lambda_{i,j} - \lambda_{i',j})} \tag{A16}$$

7-In the end, through the following equations outlet air temperature and humidity ratio equations (which are the target of this modeling) are calculated.

$$\theta_{a,out,j}(\tau) = A\,\theta_{d,avg,j}(\tau) + (1 - A)\theta_{a,in,j} \tag{A17}$$

$$\Omega_{a,out,j}(\tau) = A\,\Omega_{d,avg,j}(\tau) + (1 - A)\Omega_{a,in,j} \tag{A18}$$

References

[1] Residential Sector Canada Table 2: Secondary Energy Use and GHG Emissions by End-Use | Natural Resources Canada, (n.d.).

[2] M. Orme, Estimates of the energy impact of ventilation and associated financial expenditures, Energy Build. 33 (2001) 199–205, https://doi.org/10.1016/S0378-7788(00)00082-7.

[3] P. Nejat, F. Jomehzadeh, M.M. Taheri, M. Gohari, M.Z. Muhd, A global review of energy consumption, CO2 emissions and policy in the residential sector (with an overview of the top ten CO2 emitting countries), Renew. Sustain. Energy Rev. 43 (2015) 843–862, https://doi.org/10.1016/j.rser.2014.11.066.

[4] M. Justo Alonso, P. Liu, H.M. Mathisen, G. Ge, C. Simonson, Review of heat/energy recovery exchangers for use in ZEBs in cold climate countries, Build. Environ. 84 (2015) 228–237, https://doi.org/10.1016/j.buildenv.2014.11.014.

[5] T. Kovesi, N.L. Gilbert, C. Stocco, D. Fugler, R.E. Dales, M. Guay, J.D. Miller, Indoor air quality and the risk of lower respiratory tract infections in young Canadian Inuit children, CMAJ. 177 (2007) 155–160, https://doi.org/10.1503/cmaj.061574.

[6] ASHRAE, ASHRAE 62.1-2015 Ventilation for Acceptable Indoor Air Quality, n.d.

[7] M. Amani, S. Foroushani, M. Sultan, M. Bahrami, Comprehensive review on dehumidification strategies for agricultural greenhouse applications, Appl. Therm. Eng. 181 (2020), 115979, https://doi.org/10.1016/j.applthermaleng.2020.115979.

[8] J. Liu, W. Li, J. Liu, B. Wang, Efficiency of energy recovery ventilator with various weathers and its energy saving performance in a residential apartment, Energy Build. 42 (2010) 43–49, https://doi.org/10.1016/j.enbuild.2009.07.009.
[9] A. Mardiana-Idayu, S.B. Riffat, An experimental study on the performance of enthalpy recovery system for building applications, Energy Build. 43 (2011) 2533–2538, https://doi.org/10.1016/j.enbuild.2011.06.009.
[10] L. Wang, D. Curcija, J. Breshears, The energy saving potentials of zone-level membrane-based enthalpy recovery ventilators for VAV systems in commercial buildings, Energy Build. 109 (2015) 47–52, https://doi.org/10.1016/j.enbuild.2015.10.009.
[11] M. Sultan, T. Miyazaki, B.B. Saha, S. Koyama, Steady-state investigation of water vapor adsorption for thermally driven adsorption based greenhouse air-conditioning system, Renew. Energy. 86 (2016) 785–795, https://doi.org/10.1016/j.renene.2015.09.015.
[12] K. Ghali, Energy savings potential of a hybrid desiccant dehumidification air conditioning system in Beirut, Energy Convers. Manag. 49 (2008) 3387–3390, https://doi.org/10.1016/j.enconman.2008.04.014.
[13] C.A. Balaras, E. Dascalaki, A. Gaglia, HVAC and indoor thermal conditions in hospital operating rooms, Energy Build. 39 (2007) 454–470, https://doi.org/10.1016/j.enbuild.2006.09.004.
[14] G. Qadar Chaudhary, M. Ali, N.A. Sheikh, S.I.u.H. Gilani, S. Khushnood, Integration of solar assisted solid desiccant cooling system with efficient evaporative cooling technique for separate load handling, Appl. Therm. Eng. 140 (2018) 696–706.
[15] M. Amani, M. Bahrami, Greenhouse dehumidification by zeolite-based desiccant coated heat exchanger, Appl. Therm. Eng. 183 (2021), 116178, https://doi.org/10.1016/j.applthermaleng.2020.116178.
[16] T.S. Ge, Y.J. Dai, R.Z. Wang, Performance study of silica gel coated fin-tube heat exchanger cooling system based on a developed mathematical model, Energy Convers. Manag. 52 (2011) 2329–2338, https://doi.org/10.1016/j.enconman.2010.12.047.
[17] T.S. Ge, Y.J. Dai, R.Z. Wang, Performance study of desiccant coated heat exchanger air conditioning system in winter, Energy Convers. Manag. 123 (2016) 559–568, https://doi.org/10.1016/j.enconman.2016.06.075.
[18] A. Saeed, A. Al-Alili, A review on desiccant coated heat exchangers, Sci. Technol. Built Environ. 23 (2017) 136–150, https://doi.org/10.1080/23744731.2016.1226076.
[19] Y. Zhao, T.S. Ge, Y.J. Dai, R.Z. Wang, Experimental investigation on a desiccant dehumidification unit using fin-tube heat exchanger with silica gel coating, Appl. Therm. Eng. 63 (2014) 52–58, https://doi.org/10.1016/j.applthermaleng.2013.10.018.
[20] X.Y. Sun, Y.J. Dai, T.S. Ge, Y. Zhao, R.Z. Wang, Experimental and comparison study on heat and moisture transfer characteristics of desiccant coated heat exchanger with variable structure sizes, Appl. Therm. Eng. 137 (2018) 32–46, https://doi.org/10.1016/j.applthermaleng.2018.03.071.
[21] T.U. Erkek, A. Gungor, H. Fugmann, A. Morgenstern, C. Bongs, Performance evaluation of a desiccant coated heat exchanger with two different desiccant materials, Appl. Therm. Eng. 143 (2018) 701–710, https://doi.org/10.1016/j.applthermaleng.2018.06.012.
[22] The Modelica Association — Modelica Association, (n.d.).
[23] M. Jagirdar, P.S. Lee, Mathematical modeling and performance evaluation of a desiccant coated fin-tube heat exchanger, Appl. Energy. 212 (2018) 401–415, https://doi.org/10.1016/j.apenergy.2017.12.038.
[24] P. Vivekh, D.T. Bui, M. Kumja, M.R. Islam, K.J. Chua, Theoretical performance analysis of silica gel and composite polymer desiccant coated heat exchangers based on a CFD approach, Energy Convers. Manag. 187 (2019) 423–446, https://doi.org/10.1016/j.enconman.2019.02.093.
[25] D.-Y. Lee, D.-S. Kim, Analytical modeling of a desiccant wheel, Int. J. Refrig. 42 (2014) 97–111, https://doi.org/10.1016/j.ijrefrig.2014.02.003.
[26] H. Kang, G. Lee, D.Y. Lee, Explicit analytic solution for heat and mass transfer in a desiccant wheel using a simplified model, Energy. 93 (2015) 2559–2567, https://doi.org/10.1016/j.energy.2015.10.091.
[27] H. Kang, S. Choi, D.-Y. Lee, Analytic solution to predict the outlet air states of a desiccant wheel with an arbitrary split ratio, Energy. 153 (2018) 301–310, https://doi.org/10.1016/j.energy.2018.03.177.
[28] H. Bahrehmand, M. Ahmadi, M. Bahrami, Oscillatory heat transfer in coated sorber beds: An analytical solution, Int. J. Refrig. 105 (2019) 169–177, https://doi.org/10.1016/j.ijrefrig.2018.05.006.
[29] H. Bahrehmand, M. Ahmadi, M. Bahrami, Analytical modeling of oscillatory heat transfer in coated sorption beds, Int. J. Heat Mass Transf. 121 (2018) 1–9, https://doi.org/10.1016/j.ijheatmasstransfer.2017.12.147.
[30] H. Bahrehmand, M. Bahrami, An analytical design tool for sorber bed heat exchangers of sorption cooling systems, Int. J. Refrig. 100 (2019) 368–379, https://doi.org/10.1016/j.ijrefrig.2019.02.003.
[31] X.Y. Sun, Y.J. Dai, T.S. Ge, Y. Zhao, R.Z. Wang, Heat and mass transfer comparisons of desiccant coated microchannel and fin-and-tube heat exchangers, Appl. Therm. Eng. 150 (2019) 1159–1167, https://doi.org/10.1016/j.applthermaleng.2019.01.071.
[32] S. Chai, X. Sun, Y. Zhao, Y. Dai, Experimental investigation on a fresh air dehumidification system using heat pump with desiccant coated heat exchanger, Energy. 171 (2019) 306–314, https://doi.org/10.1016/j.energy.2019.01.023.
[33] A. Freni, B. Dawoud, L. Bonaccorsi, S. Chmielewski, A. Frazzica, L. Calabrese, G. Restuccia, Characterization of Zeolite-Based Coatings for Adsorption Heat Pumps, Springer International Publishing, Cham (2015), https://doi.org/10.1007/978-3-319-09327-7.
[34] C. Elliott, V. Vijayakumar, W. Zink, R. Hansen, National Instruments LabVIEW: A Programming Environment for Laboratory Automation and Measurement, J. Assoc. Lab. Autom. 12 (2007) 17–24, https://doi.org/10.1016/j.jala.2006.07.012.
[35] S. Kline, F. McClintock, Describing uncertainties in single sample experiments, Mech. Eng. 78 (1953) 3–8.
[36] A.A. Pesaran, A.F. Mills, Moisture transport in silica gel packed beds-I.Theoretical study, Int. J. Heat Mass Transf. 30 (1987) 1037–1049, https://doi.org/10.1016/0017-9310(87)90034-2.
[37] P.D. Dipinlal, S. Shankara Narayanan, S. Ramanathan, S. Prabhu, Experimental Investigation of Composite Desiccant Wheel Dehumidifier, Appl. Mech. Mater. 813–814 (2015) 1080–1084, https://doi.org/10.4028/www.scientific.net/amm.813-814.1080.
[38] W. Zheng, W.M. Worek, Numerical simulation of combined heat and mass transfer processes in a rotary dehumidifier, Numer. Heat Transf. Part A Appl. 23 (1993) 211–232, https://doi.org/10.1080/10407789308913669.
[39] H. Bahrehmand, M. Bahrami, Optimized sorber bed heat and mass exchangers for sorption cooling systems, Appl. Therm. Eng. 185 (2021), 116348, https://doi.org/10.1016/j.applthermaleng.2020.116348.
[40] L.J. Hua, X.Y. Sun, Y. Jiang, T.S. Ge, R.Z. Wang, Graphic general solutions for desiccant coated heat exchangers based on dimensional analysis, Int. J. Heat Mass Transf. 154 (2020), 119654, https://doi.org/10.1016/j.ijheatmasstransfer.2020.119654.
[41] D.P.D. Theodore L. Bergman, Adrienne S. Lavine, Frank P. Incropera, Fundamentals of Heat and Mass Transfer, 8th Edition | Wiley, 2017.
[42] Vaisala, Humidity conversion formulas, (n.d.).
[43] E. Cerrah, C. McCague, M. Bahrami, Sorbent based enthalpy recovery ventilator, Energy Build. 211 (2020), 109755, https://doi.org/10.1016/j.enbuild.2020.109755.
[44] L. Liu, T. Zeng, H. Huang, M. Kubota, N. Kobayashi, Z. He, J. Li, L. Deng, X. Li, Y. Feng, K. Yan, Numerical modelling and parametric study of an air-cooled desiccant coated cross-flow heat exchanger, Appl. Therm. Eng. 169 (2020), 114901, https://doi.org/10.1016/j.applthermaleng.2020.114901.